J. exp. Biol. 138, 399–411 (1988)
Printed in Great Britain © The Company of Biologists Limited 1988

BIOMECHANICS OF FROG SWIMMING

I. ESTIMATION OF THE PROPULSIVE FORCE GENERATED BY *HYMENOCHIRUS BOETTGERI*

BY JULIANNA M. GAL* AND R. W. BLAKE
Department of Zoology, University of British Columbia, Vancouver, Canada

Accepted 16 March 1988

Summary

Ciné films were used to study swimming in the frog, *Hymenochirus boettgeri* (Tornier) during near-vertical breathing excursions. The animals generally decelerated during hindlimb flexion (recovery phase) and accelerated throughout hindlimb extension (power phase). Body velocity patterns of frogs are distinct from those of other drag-based paddlers, such as angelfish and water boatman, where the body is accelerated and decelerated within the power stroke phase. The propulsive force, estimated for a single sequence from quasi-steady drag and inertial considerations, was positive throughout extension. The upper and lower bounds of this estimate were calculated by considering additional components of the force balance, including the net effect of gravity and buoyancy, and the longitudinal added mass forces associated with the body. Consideration of the force balance implies that simple drag-based propulsion may not be sufficient to explain the swimming patterns observed in frogs.

Introduction

Estimating the propulsive forces generated by the locomotor apparatus of a swimming animal can be simplified by considering the force balance for swimming at a constant velocity and level in the water column; thrust equals drag and lift equals weight. In neutrally buoyant animals, there is no need to consider lift forces during constant-level swimming. When constant forward velocity is measured, a further simplification can be made: in the non-accelerating system, thrust is equal to drag.

The force balance has been used in the study of the energetics of drag-based paddling in a variety of aquatic and semi-aquatic animals (e.g. Prange, 1976; Prange & Schmidt-Neilsen, 1970; Williams, 1983; DiPrampero *et al.* 1974, in the sea turtle, duck, mink and humans, respectively). Blake (1979, 1980) investigated drag-based propulsion in the angelfish (*Pterophyllum eimekei*) and, using blade-

* Present address: Department of Pure and Applied Biology, University of Leeds, Leeds, LS2 9JT, UK.

Key words: frog, swimming biomechanics, motion analysis, drag.

element theory, developed a general model for estimating the force, power and efficiency of drag-based paddlers (Blake, 1981). Blake (1986) developed the theory further and applied it to swimming in a water boatman (*Cenocorixa bifida*). Frogs have been categorized as drag-based paddlers (Blake, 1981; Webb & Blake, 1982), mainly because of their large webbed feet. However, the caudal placement of their hind legs indicates the potential for fluid dynamic interactions, which are not acknowledged in the blade-element model.

Some anecdotal references have been made to swimming in frogs (e.g. Porter, 1967; Beebee, 1985), but no detailed study has been made. Here, velocity and acceleration records of swimming *H. boettgeri* are made from high-speed ciné films. The velocity profiles are compared with those of other paddling animals. The average forward force generated during extension of the hindlimbs is estimated from the force balance. The calculation uses the static-body drag coefficient (Gal & Blake, 1987) and instantaneous velocity measurements to establish the quasi-steady drag experienced by the animal. The acceleration records give information about the net inertial forces acting on the frog. By addition, the total forward force can be estimated. We discuss the assumptions associated with this estimate, in particular the validity of using static drag measurements to represent the resistance of dynamic systems. We compare this estimate with force calculations based on blade-element modelling in other paddlers.

Materials and methods

Animals

Healthy animals were maintained on a diet of brine shrimp, in a 22·8-litre laboratory aquarium, equipped with a recirculating filter. The water temperature varied with the ambient room temperature (20–25°C).

Filming procedure

Frogs were filmed at 500 frames s^{-1} (Locam model 51 ciné camera) during near-vertical breathing excursions. Exposure was adjusted for the acceleration of the camera with the Locam speed curve (for model 50-0003 and 51-0003, 200′–400′ LOCAM AC, 100′ acetate film, p. 30 of the Locam Instruction Manual, Redlake Corporation, 1979).

An opaque Plexiglas partition, marked with a 0·50 cm × 0·50 cm grid, was placed in the tank, approximately 5·0 cm from and parallel to the front glass panel. The camera was fixed to the floor about 1·5–2·0 m from the front of the tank, and flanked by two 800- or 1000-W floodlamps (Berkey Beam 800 and Berkey Colortran Mini King 104–051, respectively). The grid was brought into sharp focus. The field of view was marked on the front glass panel, then bounded by two more Plexiglas partitions. Eight to ten animals were placed into this enclosed area.

When any animal swam through the field of view, the lamps and camera were activated simultaneously by a single power bar. Film (8 × 30·5 m, ASA 400

Kodak 4X) was shot, processed and inspected for good sequences. A good sequence was judged by the maintenance of a straight path in a plane parallel to this front glass panel and grid, and by the symmetry of the limb stroke. The selected sequences were analysed frame-by-frame with a photographic analysis unit (P.A.L. photographic analyser). The positions of the tip of the snout and the vent were digitized, allowing for the calculation of instantaneous snout–vent length. Four sequences were chosen for analysis.

The cumulative displacement of the tip of the vent was plotted as a function of time. A seven-point moving polynomial regression was employed to smooth the data, as follows. The first seven data points (displacement, time) were fitted to a quadratic function. A single new displacement value was generated by solving this function at the fourth time increment in the seven-point set. The first and second derivatives of this function were then determined. Evaluating these new functions at the same time increment gave the instantaneous velocity and acceleration of the vent of the animal, corresponding to the best-fit displacement. The data set was moved by picking up the next sequential point and dropping the first one of the original data set, thereby maintaining seven points. The above process was repeated throughout the entire data set, to give smooth displacement, instantaneous velocity and acceleration–time records for each animal.

Analysis

The average forward force produced by a swimming animal was estimated, using the velocity and acceleration records from sequence 1, as follows. A non-zero acceleration reflects the presence of a net force (F_{net}). F_{net} is the difference between T (the total forward force or thrust), and D (drag, the resistive force):

$$F_{net} = T - D \, . \tag{1}$$

Therefore:

$$T = F_{net} + D \, . \tag{2}$$

Drag is a function of the square of velocity:

$$D = \tfrac{1}{2}\rho S_w C_D U^2 \, , \tag{3}$$

where ρ, S_w, C_D and U are fluid density, total wetted surface area, drag coefficient and velocity, respectively. The drag coefficient of the body and hindlimbs of *H. boettgeri*, determined by drop-tank experiments, is a function of Reynolds number, *Re*:

$$C_D = 3{\cdot}64 Re^{-0{\cdot}378} \, , \tag{4}$$

(fig. 3 in Gal & Blake, 1987). In this paper, this coefficient is referred to as C_D-static. *Re*, based on the snout–vent length corresponding to a hindlimb–torso orientation similar to that of the original drop-tank tests (Gal & Blake, 1987), was calculated from:

$$Re = 10^6 \times \text{velocity}\,(\text{m s}^{-1}) \times \text{length}\,(\text{m}) \, , \tag{5}$$

(Alexander, 1971). The total wetted surface area of the animal (S_w in m^2) was

estimated by a scaling relationship based on surface area measurements of preserved frogs (geometric surface area determination, see Gal & Blake, 1987 for method):

$$S_w = 0{\cdot}188\lambda^{1{\cdot}52}\,, \tag{6}$$

where λ is snout–vent length in metres (Fig. 1). The instantaneous (quasi-steady) drag force on the swimming frog was computed and plotted as a function of time for the entire flexion–extension cycle.

F_{net} is a function of the mass (m) and acceleration (a) of the animal:

$$F_{net} = ma\,. \tag{7}$$

The mass of the frog was estimated using a scaling relationship derived from measurements of preserved specimens made on a Mettler M3 microbalance with a reproducibility of $0{\cdot}10\,\mu g$:

$$\text{mass (kg)} = 1{\cdot}031 \times 10^2\lambda^{3{\cdot}19}\,, \tag{8}$$

(Fig. 2). D and F_{net} were summed over the period of extension (defined here as being initiated by the rearward displacement of the foot) to give T. The average forward force $\bar{T}$, is:

$$\bar{T} = \frac{1}{t_p}\int_{t=0}^{t=t_p} T\,dt\,. \tag{9}$$

F_{net}, D, T and $\bar{T}$ are plotted against time in Fig. 7.

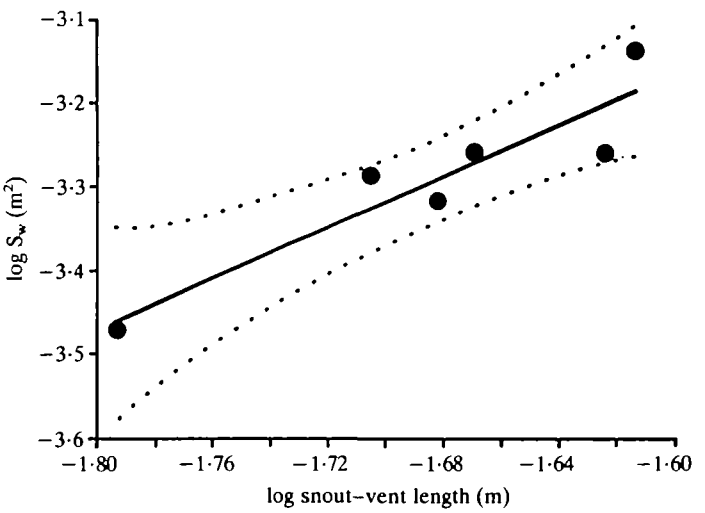

Fig. 1. Logarithm of total wetted surface area (S_w, m^2) plotted against log snout–vent length (λ, m) for preserved *Hymenochirus boettgeri*. The curve of best fit is: $\log S_w = -0{\cdot}73 + 1{\cdot}52\log\lambda$ ($N = 6$, $r = 0{\cdot}925$, $r = 0{\cdot}917$ at $P < 0{\cdot}01$). The 95% confidence intervals of the predicted S_w are $Y_i \pm t_{0{\cdot}05(2)(n-2)}S_{Y_i}$, where S_{Y_i} is the standard error of the population. S_w was measured using the geometric method of Gal & Blake (1987).

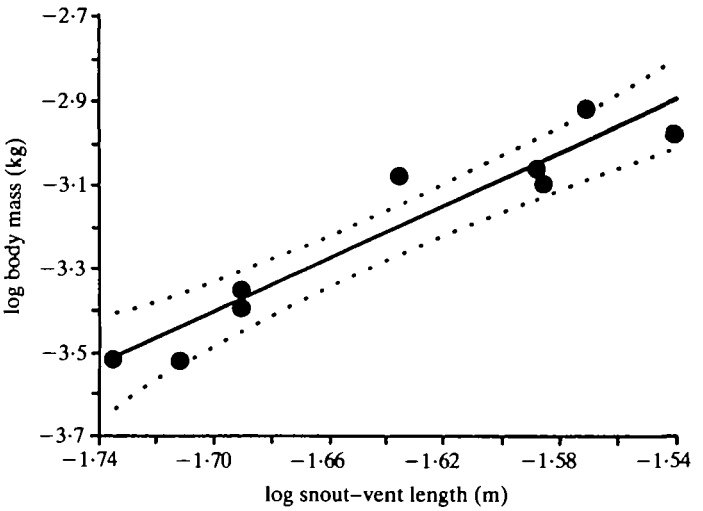

Fig. 2. Log mass (kg) plotted as a function of log snout–vent length (λ, m) for preserved *Hymenochirus boettgeri*. The curve of best fit is: log mass = 2·01+3·2logλ ($N = 9$, $r = 0{\cdot}957$, $r = 0{\cdot}898$ at $P < 0{\cdot}001$). The 95 % confidence intervals of the predicted mass are $Y_i \pm t_{0{\cdot}05(2)(n-2)} S_{Y_i}$, where S_{Y_i} is the standard error of the population.

Estimating upper and lower bounds of T and $\bar{T}$

Upper and lower bounds of T and $\bar{T}$ were estimated by considering additional components of the force balance including gravitational, buoyant and added mass forces. Because the snout–vent length was found to increase and decrease with the flexion and extension of the hindlimbs, respectively (Fig. 3D), the instantaneous velocity and acceleration of the vent (Fig. 4A and Fig. 5A, respectively) underestimate the corresponding values for the snout during extension. When this is corrected, upper (snout) and lower (vent) estimates of the instantaneous velocity and acceleration of the body can be made.

During respiratory excursions in the laboratory, these animals usually make near-vertical ascents, often releasing a gas bubble immediately before breaking the surface. The frogs then quickly gulp air and return to the substrate along virtually the same path. Buoyancy regulation occurs at the tank floor, where, if necessary, air bubbles are released until the animal remains stationary. *H. boettgeri* may be positively, neutrally or negatively buoyant during descent (as in sequence 1). Determining the buoyant state of the swimming animal is difficult. Balance readings (Mettler PK300, reproducibility 0·50 mg) were recorded from six live anaesthetized (MS 222, approximate concentration 0·17 g l^{-1}) animals both in air and completely submerged. Two animals floated, indicating positive buoyancy (not determined quantitatively). One remained on the submerged pan but did not register on the balance, indicating neutral buoyancy. Readings of three submerged animals were 1·5–7·0 % of their 'in air' values, indicating levels of negative buoyancy. The lower bounds of T and $\bar{T}$ were influenced by the maximum

recorded value of negative buoyancy (i.e. 7·0 %, the 'air' weight of the animal). Similarly, the upper bounds of T and $\bar{T}$ assumed a hypothetical positive buoyancy of 7·0 % 'air' weight.

When a body is accelerated through a fluid, a mass of that fluid is accelerated with it, effectively increasing the total mass of the system. This 'added mass' is dependent upon size, volume, shape, fluid density and type of motion (Batchelor, 1967). The frog's body was modelled as an ellipsoid, and its added mass coefficient was estimated from the relationship between the fineness ratio of technical bodies and added mass coefficients (Landweber, 1961). Here its fineness ratio is defined as snout–vent length/average of the major and minor axes of the elliptical cross-section at the morphological shoulder. Linear measurements were made of nine preserved specimens (see Gal & Blake, 1987, for preservation methods) with Vernier calipers (Mitutoyo) and the average was used for the animal shown in sequence 1 (fineness ratio $5{\cdot}5 \pm 0{\cdot}50$, $\pm$S.D., $N = 9$). The upper bounds of T and $\bar{T}$ included the effect of an added mass coefficient of 0·10. Added mass effects were neglected in estimating the lower bounds of T and $\bar{T}$.

Results

Two complete flexion–extension and two extension sequences were chosen for motion analysis. The results of the analysis and smoothing technique for sequence 1 (a complete hindlimb flexion and extension) are shown in Fig. 3. The smooth displacement parallels the experimental values (Fig. 3A). In Fig. 3B, the experimental instantaneous velocities (the numerical differentiation of the experimental displacement curve 3A) and instantaneous velocities generated from the smoothing technique are shown. The smoothed values clarify the trend. Fig. 3C shows the smoothed acceleration during flexion and extension, with the acceleration values generated from the numerical differentiation of the experimental instantaneous velocities from Fig. 3B. The smooth record clearly shows a marked positive acceleration, reaching a maximum value at about the midpoint of hindlimb extension. No clear trend is visible in accelerations derived from double differentiation of the original displacement data. The experimental and smoothed instantaneous snout–vent length for sequence 1 is shown in Fig. 3D. Snout–vent length decreases and increases by approximately 20 % throughout flexion and extension, respectively. The iliosacral morphology of pipid frogs allows the vertebral column to slide longitudinally. Snout–vent length changes of the order of 20 % have been reported (Whiting, 1961). The displacements, velocities and accelerations are based on the progression of the vent.

Fig. 4 shows the smooth instantaneous velocity records for the four selected sequences, based on the progression of the vent. The velocity of the body increases throughout hindlimb extension, to maximum values of about 10–20 cm s^{-1}. During hindlimb flexion, body velocity may decrease steadily or remain fairly constant (Fig. 4A, 4B, respectively).

In Fig. 5, the acceleration records for the four sequences (based on the

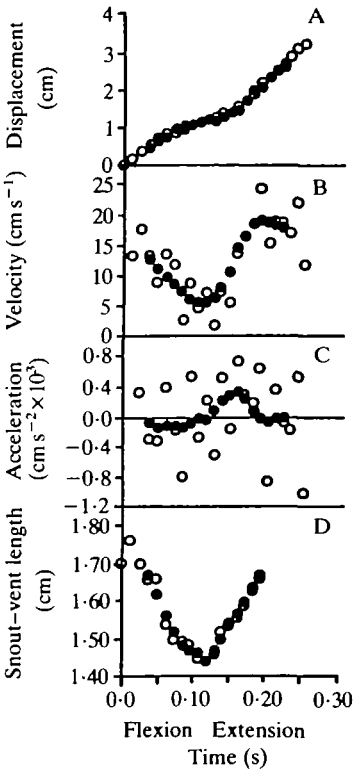

Fig. 3. The results of the motion analysis and smoothing technique for sequence 1. Experimental, and numerically differentiated data, and smoothed data are represented by open (○) and closed (●) circles, respectively.

progression of the vent) are shown. The animals accelerate throughout hindlimb extension (Fig. 5A,B,D). During the later part of extension, Fig. 5C shows a slight negative acceleration. The body may experience negative acceleration during hindlimb flexion (Fig. 5A).

C_D-static, based on the vent velocity during the hindlimb flexion of sequence 1 (Fig. 4A) and equation 4, is shown in Fig. 6 (curve A). The instantaneous force, associated with the deceleration of the body during the hindlimb flexion of sequence 1, is estimated from the acceleration values (Fig. 5A) and the body mass (equation 8). Assuming that this force is the result of static body and hindlimb drag allows the calculation of C_D-dynamic (curve B) from equation 3. The upper and lower bounds of C_D-dynamic (bounds of the stippling) were estimated by considering the upper and lower confidence limits of S_w and mass (Figs 1 and 2, respectively). Vent velocities and accelerations (Figs 4A and 5A, respectively) were used for all C_D calculations in this figure. There appears to be good correspondence between the estimates of C_D-static and C_D-dynamic during the later stages of flexion, when the hindlimbs are splayed.

The quasi-steady drag and inertial forces associated with sequence 1 are plotted

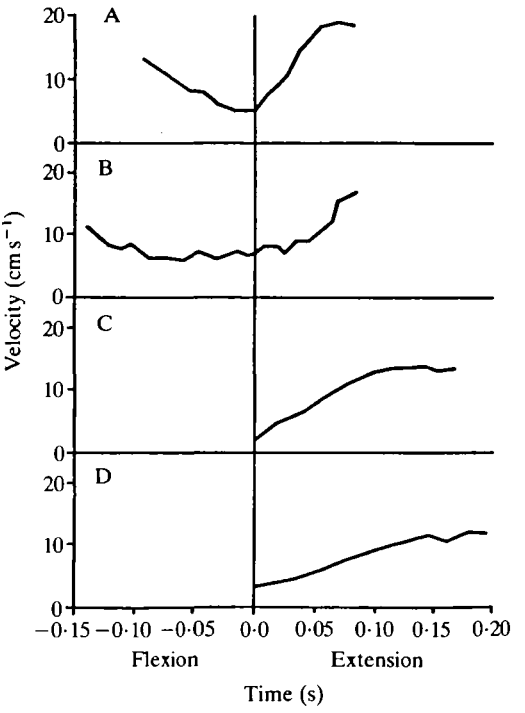

Fig. 4. Smoothed vent velocity, synchronized at hindlimb extension (defined here as being initiated by the rearward displacement of the foot), plotted as a function of time for each of the four sequences chosen for analysis.

against time in Fig. 7 (curves A and B, respectively). These two force components are summed over the period of extension to give T (bold-face curve). Upper and lower bounds of T (stippling) and $\bar{T}$ are estimated, taking account of the change in snout–vent length during hindlimb flexion and extension, the net buoyancy and gravity during breathing excursions, and the longitudinal added mass forces associated with the body. This estimate of thrust remains positive throughout hindlimb extension. The lower bound of T is further decreased if the C_D-dynamic value, corresponding to the streamlined orientation (from Fig. 6) is used to calculate the minimum quasi-steady drag, D.

Discussion

Body velocity of *H. boettgeri* increased throughout hindlimb extension (Fig. 4A,B,D), decreasing only slightly in the later stages of extension in one sequence (Fig. 4C). This pattern is consistent with the velocity record obtained by Calow & Alexander for a swimming cycle of the semi-terrestrial *Rana temporaria* (fig. 12, Calow & Alexander, 1973). It is markedly different from the velocity records of other drag-based propulsors. The angelfish, *Pterophyllum eimekei*, and water boatman, *Cenocorixa bifida*, accelerate and decelerate within the power

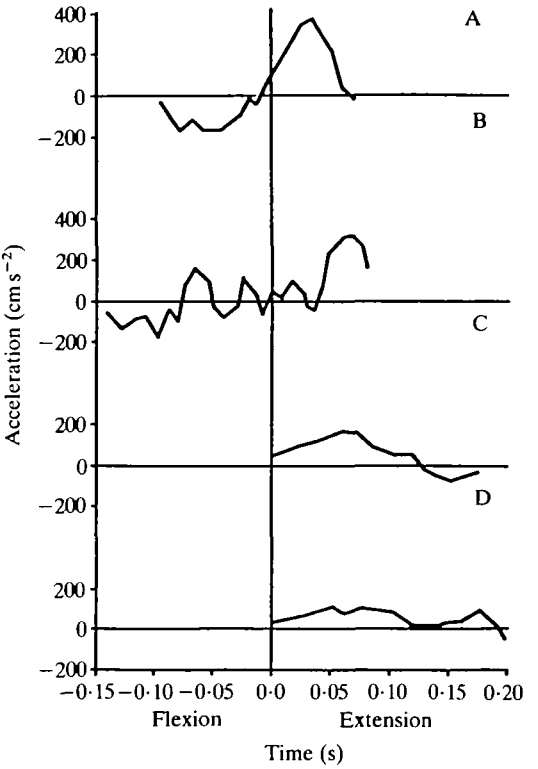

Fig. 5. Smoothed vent acceleration, synchronized at hindlimb extension (defined here as being initiated by the rearward displacement of the foot), plotted as a function of time for each of the four sequences chosen for analysis.

phase, in patterns that are dependent on Reynolds number. The angelfish (8·0 cm in length, $Re \approx 3 \times 10^3$; Blake, 1979) maintains approximately constant body velocity throughout the cycle. The water boatman (0·85 cm in length, $Re \approx 3 \times 10^2$; Blake, 1986) stops at the end of the power phase, and moves slightly backwards during recovery. This pattern is more exaggerated in the nauplii larvae (0·08 cm) of certain crustaceans (R. W. Blake, personal observation). On the basis of *Re*, one might predict that *H. boettgeri* (snout–vent length ≈ 2·0 cm) would show an oscillatory pattern between that of the angelfish and water boatman. This is not the case. Moreover, *H. boettgeri* and *R. temporaria* show a similar accelerative pattern throughout the power and recovery stroke despite at least an order of magnitude difference in *Re* (approximately $3{\cdot}0 \times 10^3$ and $3{\cdot}0 \times 10^4$, respectively). These differences suggest that a simple drag-based propulsion mechanism may not be sufficient to describe the locomotor behaviour of frogs.

An estimate of the propulsive force, T, generated during the hindlimb extension of *H. boettgeri*, is shown in Fig. 7. Despite wide bounds, T and $\bar{T}$ remain positive throughout the period of extension. Because of its streamlined profile, the added mass forces associated with accelerating the body are small (added mass

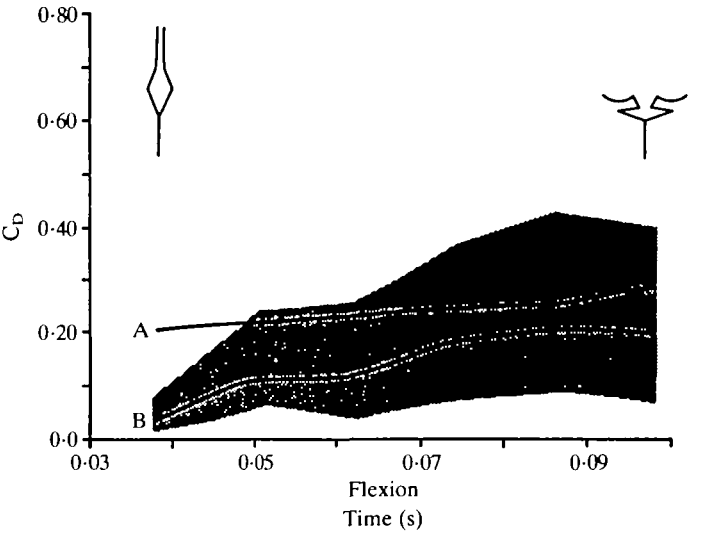

Fig. 6. C_D-static (A, calculated from equation 4 and the vent velocity) and C_D-dynamic [B, calculated from the mean decelerative force of sequence 1 (vent acceleration, mean mass)], plotted as functions of time during the hindlimb flexion of sequence 1. The upper and lower bounds of C_D-dynamic (bounds of the stippling) were estimated using the 95% confidence intervals of S_w and mass (Figs 1 and 2, respectively). Vent velocities and accelerations were used for all C_D-dynamic calculations. The stick figures indicate the orientation of the hindlimbs at the initial and final stages of flexion.

coefficient of 0·10). Additionally, buoyant forces are also likely to be small. The dominant forces which must be overcome by the propulsive efforts of this animal are inertia and drag.

Static drag measurements (C_D-static) may not reflect the resistance experienced by a swimming body. Lighthill (1975), inferred that the drag on fish swimming in the subcarangiform mode may be up to five times greater than that on a similar rigid streamlined body. Drag augmentation in fish has been reviewed by Blake (1983). Prange (1976) justified his use of static drag measurements with sea turtles because of their rigid shell, arguing that the hydrodynamic complexities inherent in such measurements on fish or aquatic mammals which change their shape as they swim do not exist in the sea turtle. Fish (1984) based his muskrat swimming energetics studies on dead drag measurements with frozen animals, because he found no appreciable flexion of the body during swimming. Many rigid-bodied animals, however, are propelled by oscillating appendages. Nachtigall (1977), commented that the moving legs of the water beetle (Dytiscidae) would slightly modify the streamlining characteristics of the trunk, but contended that the interactions would be negligible. Further, he stated that unlike undulating swimmers, whose drag/thrust-generating structures are integrated and are not easily distinguished, water beetles represent swimming systems whose hydrodynamically important structures (their swimming legs) scarcely interact. Given the

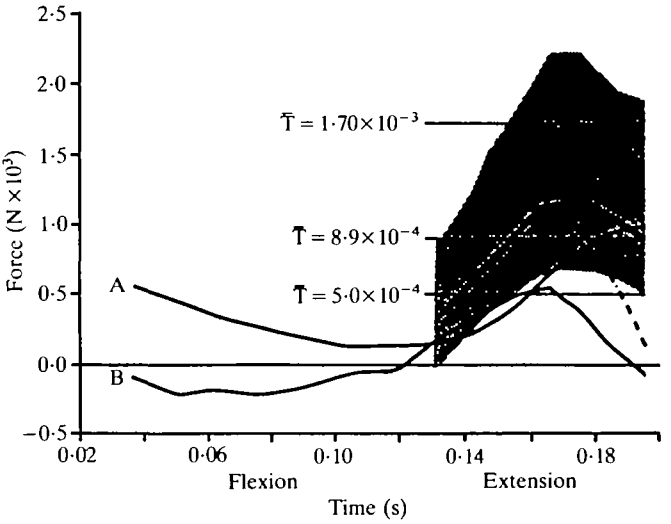

Fig. 7. The quasi-steady drag (A) and inertial forces (B) associated with sequence 1 plotted as functions of time. The predicted total thrust, T (bold line) is shown, with upper and lower bounds (stippling). The upper limit of T (upper border of stippling) and $\bar{T}$ is given by the sum of: maximum quasi-steady drag D, maximum F_{net}, a longitudinal added mass coefficient (of the body) of 0·10 and a net buoyant force of 7·0 % of the animal's maximum 'air' weight (from the upper bound of Fig. 2). The lower limit of T (lower border of stippling) and $\bar{T}$ is given by the sum: the minimum quasi-steady drag D, minimum F_{net} and a net gravitational force of 7·0 % of the animal's maximum 'air' weight. This lower limit is further decreased (dotted line) if the C_D-dynamic value corresponding to the streamlined orientation (from Fig. 6) is used to calculate the minimum quasi-steady drag, D.

delicate structure and ventrolateral placement of the swimming legs of these beetles, Nachtigall's comment seems reasonable. Blake (1986), showed that inferred C_D values for the body of the water boatman (*Cenocorixa bifida*, based on the force balance) agreed with experimentally determined drag coefficients for insects operating at similar Reynolds numbers. DiPrampero *et al.* (1974, front crawl in humans) commented that although body drag has generally been assumed to be equal to that measured on passively towed subjects, a swimmer in motion presumably experiences a higher drag, due to movements of the head, limbs and trunk, more complex wave formation, and changes in buoyancy due to respiration. Body and/or limb oscillations tend to augment drag and their relative size and orientation may significantly alter the flow about the body, relative to that of the static equivalent. Rigid-body estimates of drag probably approach real dynamic values when large rigid bodies are propelled by relatively small, steadily moving appendages.

Complications in interpreting the drag experienced by the frog are two-fold. First, the shape that the animal presents to the fluid changes with time. During extension, the frog becomes increasingly streamlined. Its frontally projected

area decreases, and the inner surfaces of the hindlimbs become shielded from the fluid. Despite an increase in velocity, drag is likely to decrease with increasing extension. Second, the development of flow changes with time. Viscous drag effects take time to develop. In unsteady flows, they increase approximately as time$^{1/2}$. Fig. 6 illustrates an attempt to contend with the first of these issues. C_D-static overestimates the dynamic resistance when the animal is streamlined, emphasizing the shape-dependence of the drag coefficient. This quasi-steady approach to quantifying the dynamic drag may be useful if a range of C_D-static values, corresponding to the hindlimb orientations throughout flexion and extension, are used. Clearly, however, the influence of shape changes and viscous flow development are difficult issues to separate when considering dynamic drag.

Sources of error in the actual calculation of T and $\bar{T}$ should be considered. F_{net} and the quasi-steady drag components required the estimation of mass and total wetted surface area (S_w), respectively. These estimates were based on scaling relationships with snout–vent length. Unfortunately, the scaling relationships were based on small samples ($N = 6$ and $N = 9$ for S_w and mass, respectively). The animal used in sequence 1 was slightly smaller than the smallest snout–vent length measurement used in the scaling curves, so back extrapolation was necessary. The 95 % confidence limits of each scaling curve are wide.

Nevertheless, the estimate of the total propulsive force generated by *H. boettgeri* (see Fig. 7) remains positive throughout hindlimb extension. Blade-element force calculations for both the angelfish and water boatman (Blake, 1979 and 1986, respectively) fall to zero or slightly negative values during the later stages of the power stroke, when the fins/legs have completed their power stroke.

It is suggested that a drag-based paddling mechanism may not be wholly sufficient to account for the thrust produced by swimming frogs. However, comparing *H. boettgeri* with animals that are propelled by the movement of rigid spar-like appendages, overlooks the complexities associated with multisegment kinematics. The caudal placement of the hindlimbs indicates the potential for interactive effects. In the following paper (Gal & Blake, 1988), the forces generated by the flexion and extension of the hindlimbs of *H. boettgeri* are calculated and compared with the locomotor behaviour recorded here.

We would like to thank the Natural Sciences and Engineering Research Council of Canada for financial support. Special thanks are due to Dr J. M. Gosline for his helpful advice on this work.

References

ALEXANDER, R. MCN. (1971). *Size and Shape*. London: Edward Arnold.

BATCHELOR, G. K. (1967). *An Introduction to Fluid Dynamics*. London: Cambridge University Press.

BEEBEE, T. (1985). *Frogs and Toads*. London: Whittet Books Ltd.

BLAKE, R. W. (1979). The mechanics of labriform locomotion. I. Labriform locomotion in the angelfish *(Pterophyllum eimekei)*: an analysis of the power stroke. *J. exp. Biol.* **82**, 255–271.

BLAKE, R. W. (1980). The mechanics of labriform locomotion. II. An analysis of the recovery

stroke and the overall fin beat cycle propulsive efficiency of the angelfish. *J. exp. Biol.* **85**, 337–342.

BLAKE, R. W. (1981). Drag-based mechanisms of propulsion in aquatic vertebrates. In *Vertebrate Locomotion* (ed. M. H. Day), *Symp. Zool. Soc., Lond.* **48**, 29–53. London: Academic Press.

BLAKE, R. W. (1983). *Fish Locomotion*. Cambridge: Cambridge University Press.

BLAKE, R. W. (1986). Hydrodynamics of swimming in the water boatman, *Cenocorixa bifida*. *Can. J. Zool.* **64**, 1606–1613.

CALOW, L. & ALEXANDER, R. MCN. (1973). A mechanical analysis of the hind leg of a frog (*Rana temporaria*). *J. Zool., Lond.* **171**, 293–321.

DIPRAMPERO, P. E., PENDERGAST, D. R., WILSON, D. W. & RENNIE, D. W. (1974). Energetics of swimming in man. *J. appl. Physiol.* **37**, 1–5.

FISH, F. E. (1984). Mechanics, power output and efficiency of the swimming muskrat (*Ondatra zibithicus*). *J. exp. Biol.* **110**, 183–201.

GAL, J. M. (1987). Biomechanics of swimming in the frog, *Hymenochirus boettgeri*. Masters thesis. University of British Columbia, Vancouver, Canada.

GAL, J. M. & BLAKE, R. W. (1987). Hydrodynamic drag of two frog species: *Hymenochirus boettgeri* and *Rana pipiens*. *Can. J. Zool.* **65**, 1085–1090.

GAL, J. M. & BLAKE, R. W. (1988). Biomechanics of frog swimming. II. Mechanics of the limb-beat cycle in *Hymenochirus boettgeri*. *J. exp. Biol.* **138**, 413–429.

LANDWEBER, L. (1961). Motion of immersed and floating bodies. In *Handbook of Fluid Dynamics* (ed. V. L. Streeter), pp. 13-1–13-50. New York: McGraw-Hill.

LIGHTHILL, M. J. (1975). *Mathematical Biofluiddynamics*. Philadelphia: Philadelphia Society for Industrial and Applied Mathematics.

NACHTIGALL, W. (1977). Swimming mechanics and energetics of locomotion of variously sized water-beetles Dytiscidae, body length 2–35 mm. In *Scale Effects in Animal Locomotion* (ed. T. J. Pedley), pp. 269–283. London: Academic Press.

PORTER, G. (1967). *The World of the Frog and Toad*. Philadelphia, New York: J. P. Lippincott Company.

PRANGE, H. D. (1976). Energetics of a swimming turtle. *J. exp. Biol.* **64**, 1–12.

PRANGE, H. D. & SCHMIDT-NIELSEN, K. (1970). The metabolic cost of swimming in ducks. *J. exp. Biol.* **53**, 763–777.

WEBB, P. W. & BLAKE, R. W. (1982). Swimming. In *Functional Vertebrate Morphology* (ed. M. Hildebrand, D. M. Bramble, K. F. Liem & D. B. Wake), pp. 110–128. Cambridge, MA: Harvard University Press.

WHITING, H. (1961). Pelvic girdle in amphibian locomotion. *Symp. zool. Soc. Lond.* **5**, 43–58.

WILLIAMS, T. M. (1983). Locomotion in the North American mink, a semi-aquatic mammal. I. Swimming energetics and body drag. *J. exp. Biol.* **103**, 155–168.